

The H α Galaxy survey[★]

IV. Star formation in the local Universe

P. A. James¹, J. H. Knapen², N. S. Shane^{1,3}, I. K. Baldry¹, and R. S. de Jong⁴

¹ Astrophysics Research Institute, Liverpool John Moores University, Twelve Quays House, Egerton Wharf, Birkenhead CH41 1LD, UK

e-mail: paj@astro.livjm.ac.uk

² Instituto de Astrofísica de Canarias, 38200 La Laguna, Spain

³ Planetary Science Group, Mullard Space Science Laboratory, Holmbury St. Mary, Dorking, Surrey RH5 6NT, UK

⁴ Space Telescope Science Institute, 3700 San Martin Drive, Baltimore, MD 21218, USA

Received 28 August 2007 / Accepted 13 February 2008

ABSTRACT

Aims. We present an analysis of the star formation properties of field galaxies within the local volume out to a recession velocity limit of 3000 km s⁻¹.

Methods. A parent sample of 863 star-forming galaxies is used to calculate a *B*-band luminosity function. This is then populated with star formation information from a subsample of 327 galaxies, for which we have H α imaging, firstly by calibrating a relationship between galaxy *B*-band luminosity and star formation rate, and secondly by a Monte Carlo simulation of a representative sample of galaxies, in which star formation information is randomly sampled from the observed subset.

Results. The total star formation rate density of the local Universe is found to be between 0.016 and 0.023 M_{\odot} yr⁻¹ Mpc⁻³ with the uncertainties dominated by the internal extinction correction used in converting measured H α fluxes to star formation rates. If our internally derived *B*-band luminosity function is replaced by one from the Sloan Digital Sky Survey blue sequence, the star formation rate densities are ~60% of the above values. We also calculate the contribution to the total star formation rate density from galaxies of different luminosities and Hubble *T*-types. The largest contribution comes from bright galaxies with $M_B \sim -20$ mag, and the total contribution from galaxies fainter than $M_B = -15.5$ mag is less than 10%. Almost 60% of the star formation rate density comes from galaxies of types Sb, Sbc or Sc; 9% from galaxies earlier than Sb and 33% from galaxies later than Sc. Finally, 75–80% of the total star formation in the local Universe is shown to be occurring in disk regions, defined as being >1 kpc from the centres of galaxies.

Conclusions. The star formation rate density estimates found here are consistent with values from the recent literature using a range of different star formation indicators. Even though they are numerous, dwarf galaxies contribute little to the star formation in the local Universe, and the bulk of the star formation takes place in L^* spirals.

Key words. galaxies: general – galaxies: spiral – galaxies: irregular – galaxies: fundamental parameters – galaxies: stellar content – galaxies: statistics

1. Introduction

In spite of many studies of the star formation (SF) process in all types of galaxy, and of the variation of the total SF rate (SFR) as a function of cosmological look-back time, many questions remain. In particular, a full census of the SF activity across all types of field galaxies, including the faintest star-forming dwarfs, is yet to be completed. The H α Galaxy Survey (H α GS) is a study of the SF properties of galaxies in the local Universe, using fluxes in the H α line to determine the total rates and distributions of SF within the selected galaxies, as a contribution to just such a census. The observations cover 334 galaxies, which sample all star-forming spiral and dwarf galaxy types (S0a – Im), and the galaxies have recession velocities less than 3000 km s⁻¹. All galaxies were observed with the 1.0 m Jacobus Kapteyn Telescope (JKT), part of the Isaac Newton Group of Telescopes (ING) situated on La Palma in the Canary Islands. The selection

and the observation of the sample are discussed in James et al. (2004, hereafter Paper I).

Since H α GS includes a large number of dwarf galaxies, which are only detectable at very small distances, the sample as it stands is not volume-limited. However, the galaxy selection was performed according to well-defined criteria in terms of galaxy apparent magnitudes, diameters and recession velocities, and so it is possible to calculate incompleteness corrections for galaxies of all types, from the fraction of the total surveyed volume in which they could lie and still satisfy the selection criteria. By applying such corrections, volume density statistics, such as luminosity functions, can be calculated. This is the primary aim of the present paper. This analysis will then enable the calculation of the average SFR density (in units of M_{\odot} yr⁻¹ Mpc⁻³) due to all galaxies, and the same quantity subdivided into the contributions from different categories of galaxy.

Thus the key scientific questions we will address are as follows:

- How does the total SFR density derived from the H α GS sample compare with other local (but generally larger-scale)

[★] Based on observations made with the Jacobus Kapteyn Telescope operated on the island of La Palma by the Isaac Newton Group in the Spanish Observatorio del Roque de los Muchachos of the Instituto de Astrofísica de Canarias.

estimates, and with estimates at intermediate and high redshifts (recently reviewed by Hopkins & Beacom 2006)?

- What fraction of the SFR density is contributed by galaxies as a function of their morphological type, and as a function of their optical luminosity?
- What fraction of the SFR density occurs within the central bulge regions of spiral galaxies, and what fraction in disks?

This approach is complementary to that adopted by other surveys of SF in the low redshift Universe (e.g. Gallego et al. 1995; Brinchmann et al. 2004) in that it samples low-luminosity spiral and irregular galaxies more fully than any previous study. The SF indicator used (narrow-band CCD imaging in the H α line) also allows good estimates of total SFRs without the need to correct for missed flux which occurs for slit- or fibre-based spectroscopy, and gives two-dimensional spatial information which is not available from such spectroscopic approaches.

The structure of the current paper is as follows. After summarising the survey data in Sect. 2, we derive, in Sect. 3, the local (*B*-band) luminosity function from the parent sample of galaxies used for the survey. This will be compared to luminosity functions from the literature derived from a comparable field sample of galaxies. In Sect. 4, the local SFR density will be calculated, first by a direct conversion of *B*-band luminosity to SFR, and secondly using a Monte Carlo method to extrapolate the properties of the observed sample of galaxies to the whole parent population from which they were drawn. In Sect. 5, the contribution to the total SFR density from galaxies of different absolute magnitudes and types is investigated. The split of SF between the central 1 kpc in radius and disk regions is explored in Sect. 6. Section 7 contains a comparison of the total SFR density estimates derived here with literature values, and all results are summarised in Sect. 8. Finally, the appendix looks at how the morphological types used in the present analysis map onto the widely-discussed red and blue galaxy sequences.

2. The galaxy sample selection

The primary aim of H α GS was to determine the total SFR of all galaxies in the local Universe, and to analyse the contributions to this total from galaxies of different types and luminosities. In particular, it was considered very important to give detailed consideration to low-luminosity dwarf galaxies, which are numerically the dominant galaxy population, but are often omitted from studies of this type. For example, the fainter galaxies are inevitably numerically under-represented in any magnitude-limited sample. In this section we describe the sample selection used to overcome these problems, which enables us to infer the total SFR of all galaxies from our observations of 327 galaxies (the remaining seven galaxies were serendipitously observed objects and are thus omitted from the analysis presented here).

The H α GS sample was selected from the Uppsala Galaxy Catalogue (UGC; Nilson 1973). We assume the UGC is complete within its selection criteria, that is, all galaxies down to a limiting diameter of 1.0' at declinations greater than -2.5° . Selection biases in the UGC are beyond the scope of this work (but see de Jong & Lacey 2000, who find incompleteness of both high and low surface brightness galaxies in the similar ESO-Uppsala catalogue; Lauberts 1982).

The H α GS selection criteria are described in detail in Paper I, but can be summarised as follows: type S0a ($T = 0$) or later; diameters between 1.7 and 6.0 arcmin and recession velocities less than 3000 km s $^{-1}$. A *B*-band magnitude limit of 15.5 was adopted, corresponding to the limiting magnitude beyond

which the UGC becomes significantly incomplete. A Galactic latitude limit of $|b| > 20^\circ$ was also imposed to minimise the effects of Galactic obscuration. In addition, to prevent the skewing of the results by the high density and special morphological characteristics of galaxies in the Virgo cluster, galaxies in regions centred on M 87 were excluded. We investigate the effects of varying the size of the excluded region in Sect. 3, but our adopted exclusion for the initial sample selection lead to a sample (which we refer to as the parent sample) of 863 galaxies. The observing list was trimmed by removing the most highly-inclined spiral galaxies ($a/b > 4.0$) since these suffer from the worst internal extinction effects and yield less information on the spatial distribution of SF than do face-on galaxies. The assumption here is that galaxy orientations are sufficiently random that no overall bias is introduced by this cut, i.e., the remaining 743 face-on galaxies are statistically representative of the full parent sample.

Recession velocities are available on the NASA/IPAC Extragalactic Database (NED) for all UGC galaxies that satisfy the diameter, apparent magnitude and type requirements for our parent sample. There is one frustrating exception, UGC 4413, which is just large and bright enough for conclusion, but has no measured recession velocity on NED. In any case, UGC 4413 is highly inclined and would be excluded from the pool of galaxies considered sufficiently face-on for potential observation. Overall, it can be considered that there is no incompleteness in the current sample due to missing recession velocities.

Within the time allocation, we observed a sub-sample of 327 galaxies from the parent sample, which sampled the full range of galaxy parameters in the parent sample. This gave us detailed SF parameters for each galaxy within this sub-sample. The analysis presented in this paper uses these parameters to supply estimates of the likely SF properties, and the scatter in these parameters, of galaxies as a function of type and absolute magnitude. These distributions are then used to populate a simulated volume of galaxies with SF properties, where the relative numbers of galaxies of different luminosities are drawn from a *B*-band luminosity function derived from our parent sample. Whilst this process is likely to be significantly in error for individual galaxies, it should give statistically reliable results when averaged over many tens or hundreds of galaxies.

The apparent blue magnitudes quoted by the NED for each galaxy were used. The NED magnitudes are generally taken from the Third Reference Catalogue of Bright Galaxies (RC3; de Vaucouleurs et al. 1991). To convert the apparent magnitudes to absolute magnitudes, distances were calculated for each galaxy using a Virgo-infall correction method based on that of Schechter (1980) and an asymptotic Hubble constant of 70 km s $^{-1}$ Mpc $^{-1}$. Such distances are very uncertain for the closest galaxies, and, where available, distances from the literature based on either Cepheid variables or the apparent magnitude of the tip of the red giant branch were used in preference. Figure 1 shows the distribution of absolute blue magnitudes (M_B) within the parent sample as a function of distance in Mpc, with the solid line showing the limiting magnitude adopted of $B = 15.5$ mag. The *B* magnitudes plotted here, and used in the following section for the calculation of visibility volumes, are not corrected for Galactic extinction. However, the *B* magnitudes used subsequently, for the calculation of the galaxy luminosity function and the estimation of global SFRs, have corrections applied based on the methods of Schlegel et al. (1998), which are also used to correct all H α measurements (see Sect. 4).

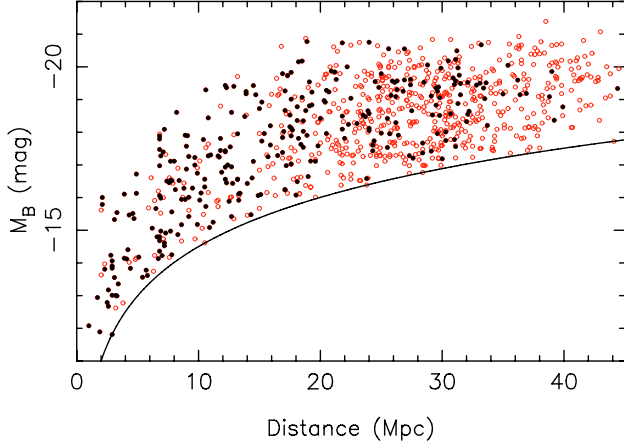


Fig. 1. The distribution of absolute blue magnitudes within the parent sample of 863 galaxies, as a function of distance in Mpc. The solid line corresponds to the apparent magnitude limit of $B = 15.5$ mag used in selecting the galaxies. Black/filled symbols denote the observed subsample, and red/open symbols the remaining unobserved galaxies.

3. The B -band luminosity function

The first stage of the analysis is to use the parent galaxy sample to produce a B -band luminosity function for galaxies in the volume sampled by this survey. We will then use the representative subsample observed in H α emission to populate this B -band function with information on SFRs of individual galaxies, from which we can calculate the total SFR in the local Universe. This two-stage process was preferred to the direct calculation of the H α luminosity function from the 327 galaxies with H α data because the latter sample is too small to constrain fully the form of the luminosity function.

The luminosity function can be most directly calculated from a volume-limited catalogue containing a fair sample of all relevant galaxies over the range of intrinsic luminosities of interest. This is not practicable, however, for the study of field galaxies over a wide range of intrinsic luminosity, as is the case with the present study; the volume over which the faintest galaxies can be seen is so small that, far from containing a fair sample of the brightest galaxies, it may contain none of them at all. In this case, it is necessary to use a statistical approach, based on the assumption that the local Universe does not differ significantly in its galaxy content and volume density from the Universe averaged over successively larger volumes. At some level, this assumption must be in error, since we live within the density enhancement of the Local Group, and close to the Virgo cluster and hence to the centre of the Local Supercluster (although the Virgo cluster galaxies themselves have been removed from the sample). This is likely to bias the calculated volume density to high values, but this is unavoidable and should be borne in mind when interpreting the results.

We use a statistical method based on the classical procedures outlined by Schmidt (1968) and by Felten (1976), to derive a B -band luminosity function from the parent sample in our present study. Mathematically, this is done by numerically weighting each of the parent sample galaxies by $(1/V_m)$, where V_m is the size in Mpc³ of the volume in which the galaxy could lie and still be included in our sample, satisfying the apparent

magnitude, diameter and recession velocity criteria. Then the luminosity function $\phi(M_B)$ is given by

$$\phi(M_B) = \frac{4\pi}{\Omega} \sum_i \frac{1}{V_m^i}. \quad (1)$$

$\phi(M_B)$ is the space density of galaxies with blue magnitude M_B , V_m^i is the visibility volume within which the i th galaxy could lie and still be included in the sample, and the quantity $\Omega/4\pi$ is the fraction of sky covered by the sample in question. In this case, $\Omega = 2\pi \times 0.695$, once the Virgo Cluster, Galactic plane and southern hemisphere regions have been removed.

Each selection criterion will define a maximum volume in which a galaxy of given properties can be observed. The visibility volume for each galaxy is thus the volume which satisfies all these criteria (Disney & Phillipps 1983; Davies et al. 1994). There are three selection limits applicable to the parent sample (apparent magnitude, diameter and recession velocity), each of which leads to constraints on the distance range within which a galaxy must lie to be included in the sample. We adopt a limiting apparent magnitude, m_{lim} , of 15.5 mag, and have excluded the small number of UGC galaxies fainter than this in defining the parent sample. A galaxy with absolute magnitude M must therefore lie within a distance in Mpc given by

$$d_{\text{max,mag}} \text{ (Mpc)} = 10^{0.2(m_{\text{lim}} - M - 25)}. \quad (2)$$

This equation applies to magnitudes uncorrected for Galactic and internal extinction. There is no bright apparent magnitude limit so $d_{\text{min,mag}} = 0$ Mpc for all galaxies. The lack of bright galaxies at distances up to 16 Mpc, clearly apparent in Fig. 1, is due to the upper diameter limit on galaxy selection, explained in the following paragraph.

The H α GS sample was selected to contain galaxies with apparent angular diameters between 1.7' and 6.0'. A galaxy with an apparent angular diameter D will be excluded from the sample if its distance, d , is low enough for the apparent diameter to be greater than 6.0', or if it is so far away that the apparent diameter falls below 1.7'. Thus the distance limits within which it can be observed are

$$d_{\text{min},D} \text{ (Mpc)} = d\left(\frac{D}{6.0}\right) \quad (3)$$

and

$$d_{\text{max},D} \text{ (Mpc)} = d\left(\frac{D}{1.7}\right). \quad (4)$$

Galaxies which are intrinsically small and faint will only be detected at the smallest distances due to the apparent magnitude and the minimum apparent diameter limits. The galaxies with the largest intrinsic sizes can only be observed at larger distances, due to the maximum angular diameter limit.

The visibility volume V_m is then defined by

$$V_m \text{ (Mpc}^3\text{)} = \frac{4\pi}{3}(d_{\text{max,lim}}^3 - d_{\text{min,lim}}^3), \quad (5)$$

where $d_{\text{max,lim}}$ is the smallest of $d_{\text{max,mag}}$, $d_{\text{max},D}$ and the distance corresponding to 3000 km s⁻¹ in the direction of the galaxy. $d_{\text{min,lim}}$ is equal to $d_{\text{min},D}$.

The B -band luminosity function is then calculated by performing the sum in Eq. (1) over all galaxies in the parent sample. The resulting function is shown in Fig. 2. The error bars contain two contributions: 1σ Poisson errors taken from the tables of

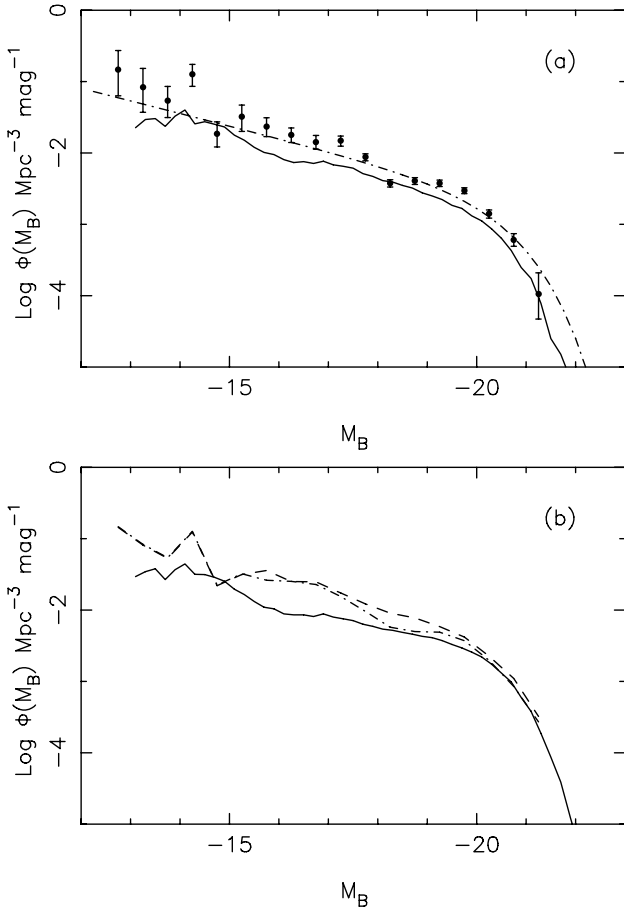


Fig. 2. **a)** The luminosity function for the entire parent sample, types S0a – Im, plotted as points with error bars; the solid line shows the luminosity function from the SDSS blue sequence. **b)** Luminosity functions including all galaxy types: SDSS (solid line); this study with all Virgo galaxies included (dashed line); and this study with galaxies excluded out to 10° from the centre of the Virgo cluster (dot-dashed line).

Gehrels (1986), which are added in quadrature to distance errors, calculated using the method of de Jong & Lacey (2000). Here we adopt distance errors of $\pm 50\%$ for all galaxies within 5 Mpc; $\pm 30\%$ for all galaxies between 5 and 10 Mpc; $\pm 20\%$ for all galaxies between 10 and 15.6 Mpc; and $\pm 15\%$ for all galaxies beyond 15.6 Mpc.

Luminosity functions of field galaxies are often found to be described well by a Schechter function (Schechter 1976) (see, e.g., Efstathiou et al. 1988):

$$\phi(L)dL = \phi^*(L/L^*)^\alpha \exp(-L/L^*)d(L/L^*), \quad (6)$$

which decreases as a power law with increasing galaxy luminosity at faint magnitudes, but cuts off sharply for galaxies brighter than some characteristic magnitude, M^* , corresponding to L^* . α gives the slope of the luminosity function at the faint end and ϕ^* sets the overall normalisation of galaxy density.

The luminosity function derived from our parent sample is shown as the points with error bars in Fig. 2a. A Schechter fit was made to this luminosity function, and is shown in Fig. 2a as the dot-dashed line. The values of M^* and ϕ^* in this fit are poorly constrained, due to the small number of galaxies brighter than the turnover at M^* and the degeneracy between these parameters. Formally, the best-fit values are $M^* = -20.49 \pm 0.19$,

$\phi^* = 0.00280 \pm 0.00062$, and the faint-end slope $\alpha = -1.44 \pm 0.06$. It should be noted, however, that a single Schechter function is not a good fit, due to the plateau in the observed function between $M_B = -18.0$ and -19.5 mag.

The solid line in Fig. 2a is an estimate of the B -band luminosity function for blue-sequence galaxies. This is derived from the Sloan Digital Sky Survey (SDSS), using the New York University Value-Added Galaxy Catalog (NYU-VAGC; Blanton et al. 2005b), in particular, the low- z galaxy sample (Blanton et al. 2005a). This sample includes galaxies with $r < 17.8$ mag in the redshift range $1000 < cz < 15\,000$ km s $^{-1}$ (14–212 Mpc assuming $H_0 = 70$ km s $^{-1}$ Mpc $^{-1}$). Galaxies have been corrected to check photometry and redshifts have been corrected to distances using a local flow model for the nearest galaxies. K -corrections are applied to bring the photometry to $z = 0$. The NYU-VAGC absolute magnitudes were converted to B magnitudes using

$$B = g + 0.14 + 0.37(g - r) \quad (7)$$

which was obtained by matching Millennium Galaxy Catalogue (MGC) galaxies (Liske et al. 2003) to SDSS galaxies and fitting a straight line to $B - g$ versus $g - r$ (using $z < 0.1$ galaxies). The SDSS luminosity function was then determined by summing, in absolute magnitude bins,

$$\frac{1}{V_{\max} C_{\text{sb}}} \quad (8)$$

where V_{\max} is obtained from the NYU-VAGC and C_{sb} is the surface-brightness completeness for each galaxy estimated using Table 1 of Blanton et al. (2005a). The luminosity function is then effectively complete to a half-light surface brightness of ~ 24 mag arcsec $^{-2}$ in r . Counts and magnitudes were all converted to $H_0 = 70$ km s $^{-1}$ Mpc $^{-1}$.

To determine the SDSS luminosity function for late type galaxies three cuts were considered: (i) a colour cut selecting blue-sequence galaxies as per Baldry et al. (2006); (ii) Sersic index less than 2.5 from the NYU-VAGC; (iii) concentration index, $R90/R50$, less than 2.5 from the SDSS pipeline. These three definitions of the blue sequence yield largely consistent luminosity functions, and we adopted the first, hereafter referred to as the SDSS blue-sequence luminosity function, to compare with that from the H α GS parent sample.

Overall there is a fair agreement in the shape and normalisation of the SDSS blue-sequence and H α GS luminosity functions, but there are two areas of significant disagreement. The first is that the H α GS luminosity function is somewhat higher around $M_B = -19.0$ to -20.5 mag, which is significant as these galaxies dominate the stellar mass and thus, plausibly, the SFR density of the overall galaxy population. Secondly, the H α GS luminosity function shows a somewhat steeper faint-end rise, i.e., a larger dwarf-to-giant ratio than the SDSS function. The possible causes of these differences will now be investigated.

One possibility is that the higher amplitude of our luminosity function is due to the presence of the Virgo cluster, which may still have a significant influence even though the core region is excluded. This possibility was explored by producing luminosity functions for local galaxies selected from the UGC, with differently-sized regions of the Virgo cluster removed. For ease of comparison with literature studies, this comparison was done for all Hubble types, i.e. with types earlier than S0a reinstated, but otherwise the selection criteria are as described above. Two luminosity functions derived in this way are shown in Fig. 2b, where the dashed line includes all Virgo cluster galaxies, and the

dot-dashed line shows the effect of excluding all galaxies within a 10° radius centred on M 87. (5° , 15° and 20° radius regions were also investigated, with similar results). For comparison, the full SDSS luminosity function, including all galaxy types, is shown as the solid line. The main effect of Virgo exclusion on the UGC luminosity function is to depress it between M_B values of -18 and -20 , thus causing the plateau mentioned above. The bright end of the function is then in fair agreement with the SDSS-derived luminosity function. At $M_B = -20$, the UGC-derived function has a value $\phi(-20)$ of $0.0031 \text{ Mpc}^{-3} \text{ mag}^{-1}$ with Virgo included, falling to 0.0029 , 0.0027 , 0.0027 and $0.0025 \text{ Mpc}^{-3} \text{ mag}^{-1}$ for excluded regions of radius 5° , 10° , 15° and 20° respectively. For the full SDSS-derived luminosity function, $\phi(-20)$ is $0.0024 \text{ Mpc}^{-3} \text{ mag}^{-1}$. This improved agreement shows that at least part of the bright-end discrepancy in Fig. 2a is due to the SDSS blue sequence definition excluding a larger fraction of galaxies than our S0a – Im type constraint. This is supported by the analysis presented in the appendix, which shows that the blue sequence most nearly corresponds to types Sb or later.

The literature sample most comparable to our parent sample is that of [Santiago et al. \(1996\)](#), who studied the luminosity and diameter functions of galaxies within 8000 km s^{-1} selected from both the UGC and its southern counterpart, the ESO-Uppsala Survey ([Lauberts 1982](#)). They do not present Schechter function fit parameters for their luminosity functions, citing significant biases in the sample selections which are hard to quantify, but the $\phi(-20)$ values for their luminosity functions from both catalogues are somewhat lower than those we derive, at 0.0019 – $0.0021 \text{ Mpc}^{-3} \text{ mag}^{-1}$, after correction from their assumed Hubble constant of $100 \text{ km s}^{-1} \text{ Mpc}^{-1}$.

It is clear from this analysis that cosmic variance may have a significant effect on the H α GS luminosity function over the volume we survey, and this will be more important at the faint end, due to the even smaller region sampled by the faintest galaxies. In order to quantify this faint-end difference, estimates were made of the amplitude of the B -band LF at $M_B = -16.0$, for comparison with literature studies. With all galaxy types and the Virgo cluster included, our UGC-based sample gave a value for $\phi(-16)$ of $0.030 \text{ Mpc}^{-3} \text{ mag}^{-1}$ falling to $0.025 \text{ Mpc}^{-3} \text{ mag}^{-1}$ with the exclusion of the Virgo cluster, and to $0.020 \text{ Mpc}^{-3} \text{ mag}^{-1}$ with the additional exclusion of galaxies earlier than type S0a. The SDSS and [Santiago et al. \(1996\)](#) luminosity functions are significantly lower in this region, with $\phi(-16)$ values between 0.006 and $0.011 \text{ Mpc}^{-3} \text{ mag}^{-1}$. Thus cosmic variance seems likely to have a substantial effect at these faint magnitudes.

However, it is also true that the larger-scale surveys have substantial incompleteness below $M_B \sim -16$ mag, and the corresponding uncertainties make it impossible to rule out the higher faint end counts that we find in the current sample. Indeed, some other studies of the local galaxy luminosity function support a faint end slope as steep as, or steeper than, that found here for the H α GS parent sample. For example, [Marinoni et al. \(1999\)](#), studying an all-sky sample of 6400 optically selected galaxies within 5500 km s^{-1} , found a very steeply-rising faint end slope ($\alpha < -2$ for the faintest galaxies, vs. ~ -1.1 over most of the luminosity range studied) with the steepening at $M_B \sim -15$ mag being ascribed to Magellanic irregular galaxies.

In light of these uncertainties in the form of the local field galaxy luminosity function, for the remainder of this paper we will adopt the H α GS and SDSS blue sequence luminosity functions as limiting cases, and use both when characterising the SF properties of the local Universe.

4. The local SFR density

4.1. Methods for estimating the SFR density from the B -band luminosity function

The B -band luminosity function calculated in the previous section from our parent sample gives the total number of galaxies of different luminosities per unit volume of the Universe. The next stage of this analysis is to populate the individual galaxies making up this luminosity function with SF information, thus enabling calculation of the total SFR density, and the breakdown of this total by galaxy type. The SF information is provided by the observed subsample of H α GS galaxies.

Two methods are presented here. The first uses galaxy B -band luminosity as a direct proxy for SFR, with calibration factors linking the two quantities being derived from the observed subsample, and applied to the full parent sample. The scatter in this conversion process is significant, however, and there are possible concerns that taking mean properties of galaxies may underestimate the effects of outliers in the distributions of SF properties. These problems are addressed with the second method, which uses a Monte Carlo method to build multiple models of the Universe, with galaxy types and luminosities drawn from the parent sample, and SF information randomly sampled from galaxies with similar properties in the observed subsample.

The H α fluxes are converted to SFR values using the calibration of [Kennicutt \(1998\)](#), which assumes a [Salpeter \(1955\)](#) stellar initial mass function.

4.2. The SFR: L_B correlation

The first of these two methods relies on the fact that B -band luminosity (L_B) in star-forming galaxies largely comes from the young stellar population, and hence we can expect galaxy L_B values to correlate strongly with SFRs. This leads to a simple way to calculate the total SFR density: we calibrate the SFR: L_B relation from the observed subsample, then use it to replace the L_B of each galaxy in the parent sample with a SFR. Finally, the same $1/V_{\text{max}}$ analysis as was used to calculate the B -band luminosity function will now result in the total SFR density.

Figure 3 shows the log of galaxy SFRs per unit B -band luminosity (in solar units), plotted against the log of the B -band luminosities, with different symbols showing early Hubble types (T -type 0–2; circled points), intermediate types (T -type 3–7; stars) and late types (T -type 8–10; filled circles). All measured fluxes are corrected for Galactic extinction, and the SFRs have been corrected for extinction internal to the galaxy concerned using the type-dependent corrections derived in Paper II ([James et al. 2005](#)). Overall, Fig. 3 shows no strong trend, confirming that B -band luminosity can be used as a proxy for SFR, but it is clear that, for example, the bright, early type galaxies have a lower mean ratio than is typical of other galaxies. Thus, calibration factors were calculated for each of these three type bins ($T = 0$ –2, 3–7 and 8–10) and three L_B bins (Faint, $\log(L_B) < 8.5$; Intermediate, $8.5 < \log(L_B) < 9.5$; and Bright, $\log(L_B) > 9.5$). In each case, the values were calculated by dividing the sum of the galaxy SFRs by the sum of their B -band luminosities in solar units, and finally taking the log. The resulting values are given in Table 1.

It is now simple to convert the L_B values for each of the parent sample galaxies to SFR, by multiplying by the calibration factor for the appropriate type and luminosity bin. Applying a $1/V_m$ weighting and summing over the whole sample, we find

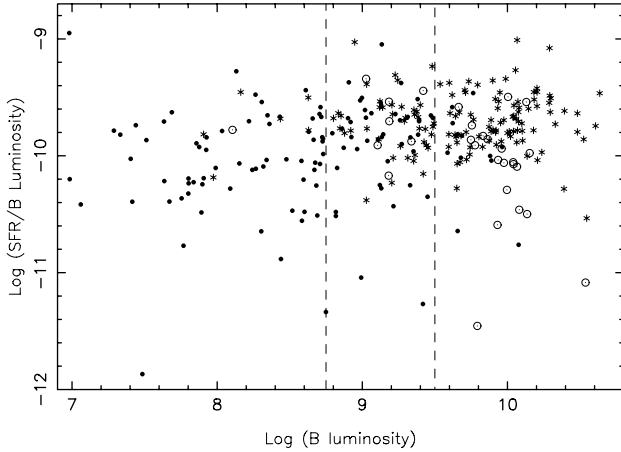


Fig. 3. The log of the SFR to B -band luminosity ratio, plotted against the log of the B -band luminosity, for the observed galaxies. Circled points denote early types, $T = 0-2$; stars are intermediate types, $T = 3-7$; and filled circles are late types, $T = 8-10$.

Table 1. $\log(\text{SFR}_{\text{TOT}}/L_{B,\text{TOT}})$ values for observed sample galaxies, binned by luminosity and Hubble T -type.

	Faint	Intermediate	Bright
$T = 0-2$	-9.78	-9.63	-10.00
$T = 3-7$	-9.64	-9.67	-9.63
$T = 8-10$	-9.88	-9.74	-9.91

the SFR density to be $0.0237 \pm 0.0030 M_{\odot} \text{ yr}^{-1} \text{ Mpc}^{-3}$. Here the quoted error is the random error resulting from uncertainties in the individual galaxy H α fluxes (James et al. 2004) and distances, and Poisson errors on the numbers of galaxies used in calculating mean binned properties. Much larger systematic uncertainties result from the extinction corrections applied in the conversion of H α fluxes to SF rates, and from the luminosity function used. These factors will be addressed in the remainder of this section.

We will next find the SFR density that results from using the SDSS blue sequence luminosity function. Again the method employed was to replace L_B with SFR values from our observed galaxy sample. However, in this case we only have the B -band luminosity function, and no information on the fraction of galaxies of each Hubble type within each L_B bin. Therefore, we calculate the (SFR/L_B) calibration factors simply as a function of L_B within our observed subsample. Since the sample is not subdivided by types, we can bin more finely in L_B , and so the mean calibration factors are calculated within nine bins of width 0.4 in $\log L_B$. The SFR density from the SDSS B -band luminosity function using this “direct” calculation method is $0.0138 \pm 0.0015 M_{\odot} \text{ yr}^{-1} \text{ Mpc}^{-3}$.

This is significantly lower than the value from the internally-derived luminosity function, due to the overall lower level of the SDSS luminosity function.

4.3. A Monte Carlo method for deriving the SFR from the B -band luminosity function

There is a concern that the above method implicitly assumes a perfect correlation between B -band luminosity and current SFR; this is clearly not a valid assumption, and even within our type-luminosity bins, the scatter in (SFR/L_B) is large, at 0.3 dex. We have investigated the possible effects of this scatter using

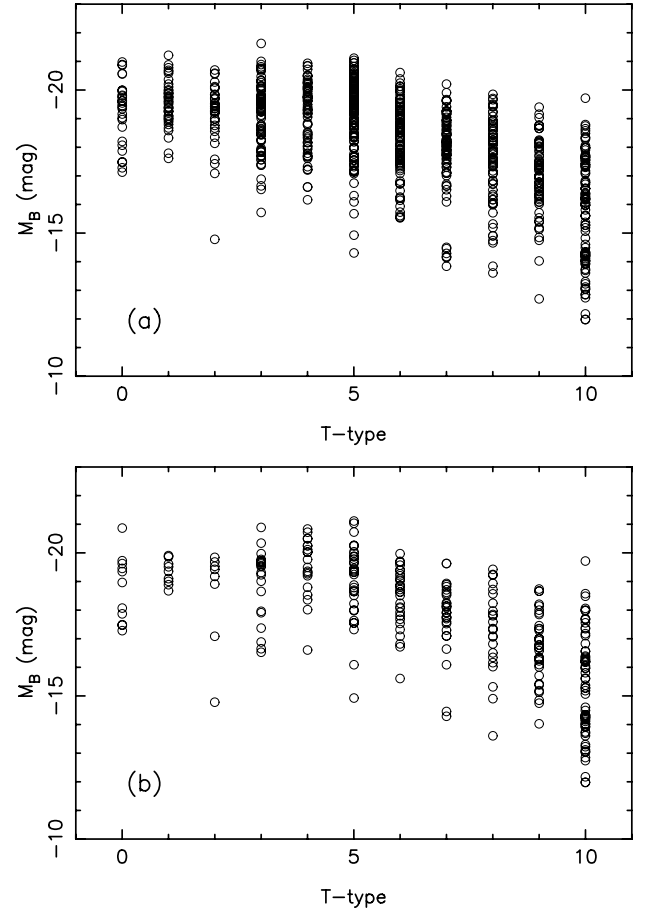


Fig. 4. The distribution of absolute magnitudes amongst each galaxy T -type for both the parent **a)** and the observed **b)** samples.

a Monte Carlo method, producing multiple realisations of the local Universe. These models were populated using the $1/V_m$, T -type, and M_B information for each of the 863 galaxies in the parent sample. The $1/V_m$ value gives the number of times each galaxy is reproduced in the model universe. For each of these reproduced galaxies, a SFR is selected by randomly sampling a galaxy from the observed subset with closely matching M_B and identical T -type (we use three M_B bins for each T -type; the selected galaxy can be any of the observed galaxies in same bin) and using the corresponding SFR.

This method requires the parent and observed samples to have well-matched properties at each T -type, so that every parent galaxy can have SF information supplied from an observed galaxy with similar characteristics. Figure 4 shows the distribution of B -band absolute magnitudes for each T -type for both parent and observed samples, showing that indeed the distributions are well-matched, as would be expected given that 40% of the full sample were observed with a good spread over all T -types. Kolmogorov-Smirnov (K-S) tests applied to each galaxy type show that the observed sample is consistent with being drawn randomly from the parent sample.

The following results for the total SFR density were obtained from the Monte Carlo analysis. Using the B -band luminosity function derived from the parent sample and type-dependent extinction corrections from Paper II in converting H α fluxes to SFRs, the SFR density is $0.0229 \pm 0.0016 M_{\odot} \text{ yr}^{-1} \text{ Mpc}^{-3}$. Using the SDSS blue-sequence B -band luminosity function, with the same H α extinction corrections, this value is reduced

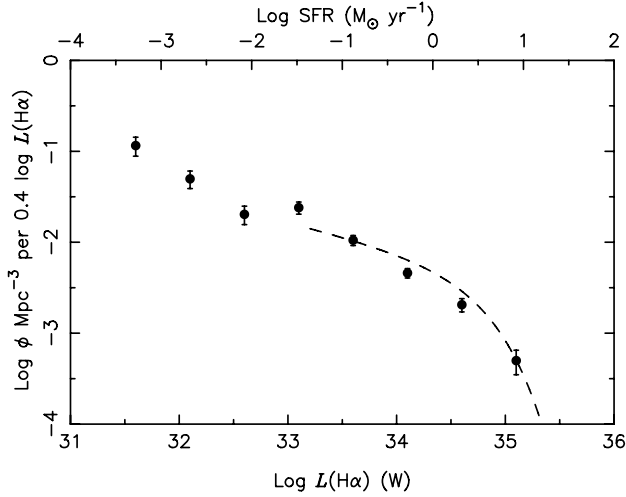


Fig. 5. The H α luminosity function derived from our parent sample, with type-dependent extinction corrections. The dashed line shows H α luminosity function of Gallego et al. (1995). The horizontal scale is given both in terms of Log (H α) luminosity, in Watts (*bottom scale*), and Log (SFR), in solar masses per year (*top scale*).

to $0.0130 \pm 0.0009 M_{\odot} \text{ yr}^{-1} \text{ Mpc}^{-3}$. In both cases, the scatter in values found using repeated realisations of the Monte Carlo method are less than the formal errors, which are dominated by Poisson statistics on the size of the observed samples. It is encouraging to note that in both cases, the Monte Carlo method gives SFR density values within a few percent of those found using the SFR: L_B correlation.

The H α luminosity function derived from our B -band luminosity function, and with the type-dependent extinction corrections, is shown in Fig. 5. For comparison, the H α luminosity function of Gallego et al. (1995) is overplotted as a dashed line, showing good agreement in overall level over the range of SFR probed by Gallego et al. (1995).

We next used the Monte Carlo technique to evaluate the effect of different H α extinction corrections on the derived SFR density, using the B -band luminosity function from the parent sample of the present study. Replacing the type-dependent correction with the constant 1.1 mag correction proposed in Kennicutt (1998) gives a SFR density of $0.0203 \pm 0.0014 M_{\odot} \text{ yr}^{-1} \text{ Mpc}^{-3}$. A third option is the M_R -dependent extinction correction derived by Helmboldt et al. (2004) based on the study of a 21 cm-selected galaxy sample (we also use their [NII] contamination correction, for consistency). This gives rather lower SFRs for a given H α flux, and a total SFR density of $0.0159 \pm 0.0012 M_{\odot} \text{ yr}^{-1} \text{ Mpc}^{-3}$. Thus the systematic uncertainties associated with internal extinction corrections are $\pm 20\%$, and much larger than the formal statistical errors.

5. The contribution of galaxies of different types and luminosities to the local SFR density

5.1. SFR density as a function of galaxy luminosity

Using the Monte Carlo method described in the previous section, it is simple to evaluate the contributions to the local SFR density from galaxies of different absolute magnitudes. This is of interest given the relatively large number of dwarf galaxies in the present sample, which could potentially offset the low individual SFRs of these dwarfs.

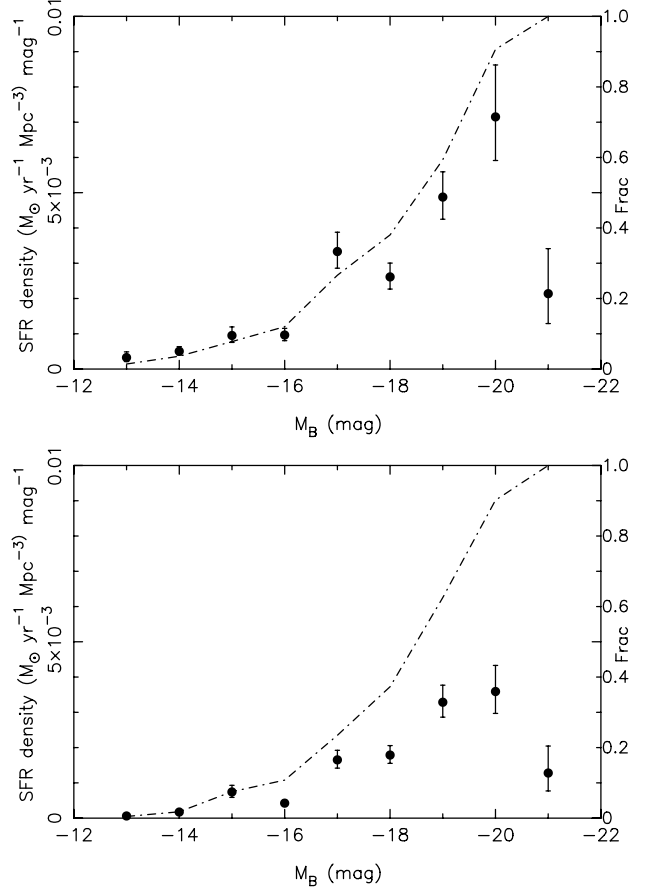


Fig. 6. SFR density as a function of absolute blue magnitude found using the points in the B -band luminosity function shown in Fig. 2 (*top*); and using the SDSS B -band luminosity function (*bottom*). The cumulative fraction of the SFR density is shown by the dot-dashed line in each plot; the scale for this fraction is marked along the *right-hand axis*.

This calculation was done using both the B -band luminosity function derived from our parent sample, and that of the SDSS blue sequence. The results are shown in Fig. 6, from which it is clear that the local SFR density is dominated by bright spiral galaxies with $M_B \sim -19$ – -20 mag, regardless of which luminosity function is used. Even with our relatively dwarf-rich luminosity function, only 8% of the SF in the local Universe is occurring in dwarf galaxies fainter than $M_B = -15.5$ mag; using the SDSS blue-sequence luminosity function this falls to 6%.

5.2. SFR density as a function of galaxy type

We can also use our Monte Carlo method to explore the fraction of the total SFR density contributed by galaxies of different types. This uses a similar method to that in the previous Sect. 5.1, but makes use of the T -type information that is available for all galaxies in the parent sample used in this simulation.

The results are shown in Fig. 7, which shows that the galaxies contributing the most to the local SF are those classified as Sb – Sc. Early type spirals provide only a small contribution in the present epoch, in spite of including many of the highest mass spiral galaxies. It is interesting to note the large step in SFR density between $T = 2$ and 3 (Sab and Sb), since these types also straddle the transition between the SDSS red and blue sequences, as explained in Appendix A. Late-type Magellanic galaxies of types Sm and Im ($T = 9$ and 10), which are the most

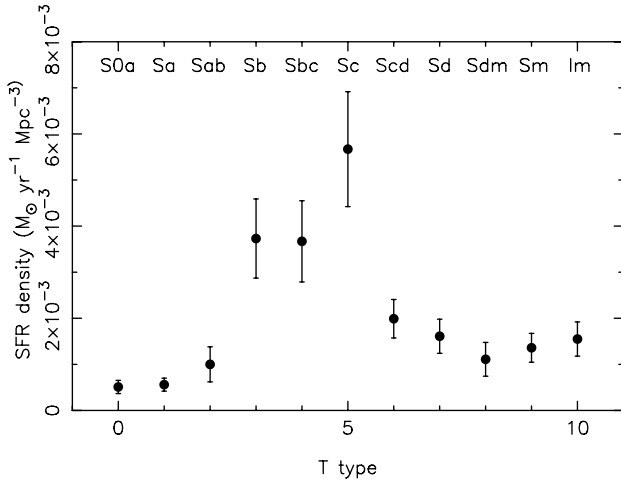


Fig. 7. SFR density as a function of galaxy morphological type, with galaxy numbers drawn from our B -band luminosity function.

numerous galaxies in the field, contribute $\sim 13\%$ (our B -band luminosity function) or $\sim 10\%$ (SDSS luminosity function) of the local SFR density.

6. Disk vs. central SF

A final study, made possible by the spatial coverage and resolution of the H α imaging technique, is to separate out SF taking place in central and disk regions of the galaxies observed. In this first analysis, we do not attempt a bulge-disk deconvolution of the galaxies, but simply define the central region (“bulge”) as being the central 1 kpc in radius (following, e.g., Galaz et al. 2006), with “disk” SF being traced by the H α emission lying outside this radius. For inclined galaxies, elliptical apertures with semi-major axis 1 kpc and axial ratios matching those of the outer disk were used, as discussed in Paper I. Disk and bulge fractions of SF were calculated in this way for all galaxies of types S0a – Sdm in our observed sample; the latest-type galaxies (Sdm, Sm and Im) are deemed to be bulge-free, and hence the disk fraction for these galaxies is 100% by definition.

One reason for doing this analysis is that the disk emission thus defined can confidently be interpreted as being dominated by SF. The bulge component can potentially be contaminated by AGN-related emission, and this process puts an upper limit on the potential over-estimate of our SFR density values from this cause. Similarly, central regions can be affected by high [NII]/H α ratios (Paper II and references therein), which can again lead to over-estimates of SFRs. On the other hand, by interpreting all the emission (bulge and disk) as being due to H α from SF, we can derive an estimate of the relative rates of growth of the stellar mass of the two components in the current epoch, bearing in mind that the bulge estimates are likely to be upper limits.

We find the following disk percentages of the local SFR density as a function of galaxy T -type: $T = 0$, 63%; $T = 1$, 54%; $T = 2$, 73%; $T = 3$, 64%; $T = 4$, 76%; $T = 5$, 83%; $T = 6$, 81%; $T = 7$, 78%. Types $T = 8$ –10 are defined to have disk SF fractions of 100% (pure disk systems). The total fraction of the SFR density occurring within disks is 75% for types 0–7; this increases to 80% when including the SF of the later type galaxies in the disk total. This demonstrates that the major part of the SF activity is occurring in disk regions, and hence that our estimates of the total SFR density cannot be significantly affected by an

AGN contribution. The bulge fraction of line emission for the earliest-type galaxies is high, however, at almost 50% of the total. This may imply that these galaxies are still building the stellar mass in their central regions at a significant rate, or it may be the result of substantial contamination from AGN or other non-SF related emission.

A fuller investigation of the spatial distribution of line emission within these galaxies will be described in a later paper in this series (James et al., in preparation).

7. Comparison with other determinations of SFR density

We finally compare our estimates of the local SFR density with estimates of this same parameter from the literature, where the latter studies use a variety of field galaxy samples and tracers of galaxy SFRs. The present study found values of this parameter ranging from 0.0159 to 0.0229 $M_{\odot} \text{ yr}^{-1} \text{ Mpc}^{-3}$ using the internally-derived B -band luminosity function, with the range reflecting the different internal extinction corrections used. Using the B -band luminosity function for the SDSS blue sequence gave a lower estimate, of 0.0130 $M_{\odot} \text{ yr}^{-1} \text{ Mpc}^{-3}$.

Literature results in this area have recently been surveyed by Hanish et al. (2006), who quote results from several surveys, with and without extinction corrections, and with and without a redshift correction, since the surveys quoted have mean effective redshifts from 0.01 to 0.20. The numbers presented here include both extinction correction and the redshift correction to bring the SFR densities to an equivalent at $z = 0$.

Two results come from the Universidad Complutense de Madrid survey of optically-selected emission line galaxies, with Gallego et al. (1995) finding a value of $0.0112 \pm 0.001 M_{\odot} \text{ yr}^{-1} \text{ Mpc}^{-3}$, and Pérez-González et al. (2003) $0.0229 \pm 0.001 M_{\odot} \text{ yr}^{-1} \text{ Mpc}^{-3}$. The I -band selected Canada-France Redshift survey of Tresse & Maddox (1998) resulted in a SFR density value of $0.0186 \pm 0.0032 M_{\odot} \text{ yr}^{-1} \text{ Mpc}^{-3}$, corrected from an effective mean redshift of 0.2 to $z = 0$. Sullivan et al. (2000) use a UV-selected sample of galaxies over quite a wide redshift range (0–0.4) to derive a SFR density of $0.01 \pm 0.001 M_{\odot} \text{ yr}^{-1} \text{ Mpc}^{-3}$, although this low value is completely dependent on the redshift correction adopted by Hanish et al. (2006). Easily the most extensive study in terms of numbers of galaxies included, is the SDSS-based study of Brinchmann et al. (2004), who find a SFR density of $0.0219^{+0.0016}_{-0.0048} M_{\odot} \text{ yr}^{-1} \text{ Mpc}^{-3}$. Finally, for their own, HI-selected field sample, Hanish et al. (2006) find a SFR density of $0.0155 \pm 0.001 M_{\odot} \text{ yr}^{-1} \text{ Mpc}^{-3}$. Overall, the range of values found is in good agreement with those derived in the current paper, and there is no clear reason to favour either the high values we obtain with the H α GS luminosity function, or the lower SDSS-derived value.

8. Summary

We have presented an analysis of the SF properties of field galaxies within the local volume out to a recession velocity limit of 3000 km s $^{-1}$. A parent sample of 863 galaxies with well-defined Hubble type, apparent magnitude and diameter limits was selected from the UGC, and used to calculate a B -band luminosity function. This was then populated with SF information from a subsample of 327 galaxies, for which we have H α imaging, firstly by calibrating a relationship between galaxy B -band luminosity and SFR, and secondly by a Monte Carlo simulation of a representative sample of galaxies, in which SF information was

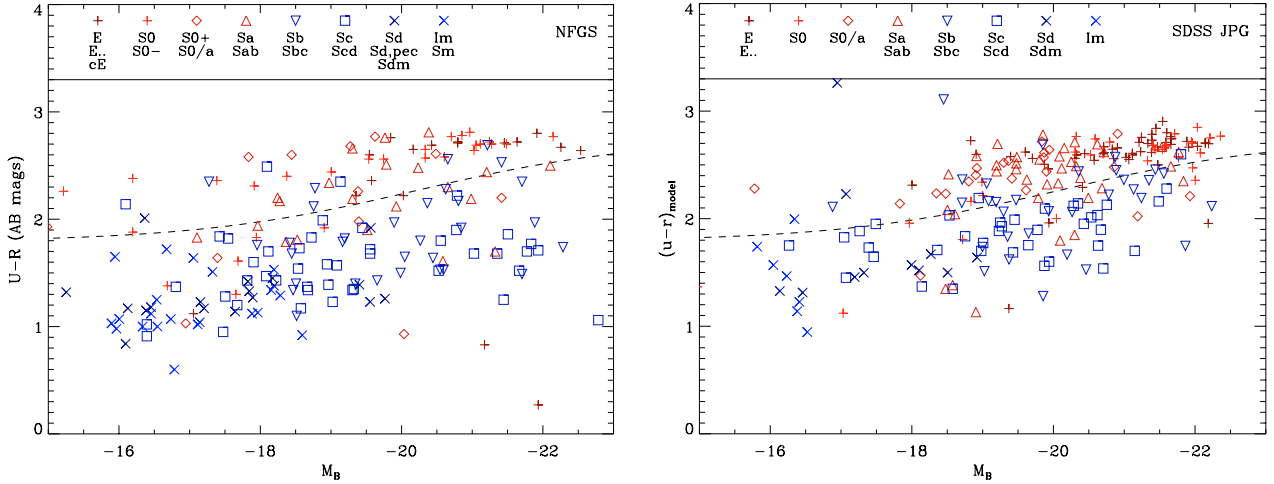


Fig. A.1. Morphological classifications in the CMD for galaxies. *Left:* NFGS sample. *Right:* a subset of the JPG sample. The dashed line in both plots represents an optimal divider between the red and blue sequences determined from a larger SDSS sample.

randomly sampled from the observed subset. The total SFR density of the local Universe was found to be between 0.016 and $0.023 M_{\odot} \text{ yr}^{-1} \text{ Mpc}^{-3}$ regardless of which of these two methods was used, with the uncertainties being dominated by the internal extinction correction used in converting measured $H\alpha$ fluxes to SF rates. If our internally derived B -band luminosity function is replaced by one from the SDSS blue sequence, the SFR densities are systematically reduced to about 60% of the above values. This range of estimates is consistent with values from the recent literature using a range of different SF indicators.

The Monte Carlo method was then used to calculate the contribution to the total SFR density from galaxies of different luminosities and Hubble T -types. The largest contribution comes from bright galaxies with $M_B \sim -20$ mag, and the total contribution from galaxies fainter than $M_B = -15.5$ mag is less than 10%. Almost 60% of the SFR density comes from galaxies of types Sb, Sbc or Sc; 9% from galaxies earlier than Sb and 33% from galaxies later than Sc. Finally, 75–80% of the total SF in the local Universe is shown to be occurring in disk regions, defined as being >1 kpc from the centres of galaxies.

Acknowledgements. The Jacobus Kapteyn Telescope was operated on the island of La Palma by the Isaac Newton Group in the Spanish Observatorio del Roque de los Muchachos of the Instituto de Astrofísica de Canarias. This research has made use of the NASA/IPAC Extragalactic Database (NED) which is operated by the Jet Propulsion Laboratory, California Institute of Technology, under contract with the National Aeronautics and Space Administration. We thank the referee for a thoughtful and helpful reading of the paper, which resulted in significant improvements in content and presentation.

Appendix A: Morphological classification along the red and blue sequences

With the advent of large imaging surveys, both local and at high redshift, colour classification in particular dividing into a red and blue sequence is often preferred to morphological classification. This is partly because of the reliability of determining galaxy colours automatically compared to morphological characteristics for these surveys, and partly because of the colour bimodality (Strateva et al. 2001). Galaxies divide naturally into a red and blue sequence when viewed in a colour–magnitude diagram (CMD) using $u - r$, $g - r$ colours or similar (Blanton et al. 2003; Baldry et al. 2004). In order to outline the connection between traditional morphological classification using the E-S0-Sa-Sd-Im scheme and the colour sequences, we used

data from the Nearby Field Galaxy Survey (NFGS; Jansen et al. 2000) and the SDSS Japanese Participation Group (JPG) catalogue (Fukugita et al. 2007).

The NFGS includes UBR surface photometry for 198 galaxies with a median redshift of 0.01. The NFGS was selected from the Huchra et al. (1983) catalogue, excluding the Virgo cluster, with sampling to obtain a maximum of about 30 galaxies per 1-mag bin (blue absolute magnitude). We used the $U - R$ colours within the effective half-light radius in B , converted to AB magnitudes (+0.55), and used the absolute B -band magnitude converted to $H_0 = 70 \text{ km s}^{-1} \text{ Mpc}^{-1}$. Figure A.1 (left) shows the CMD for these data with different symbols representing morphological classification in eight groups.

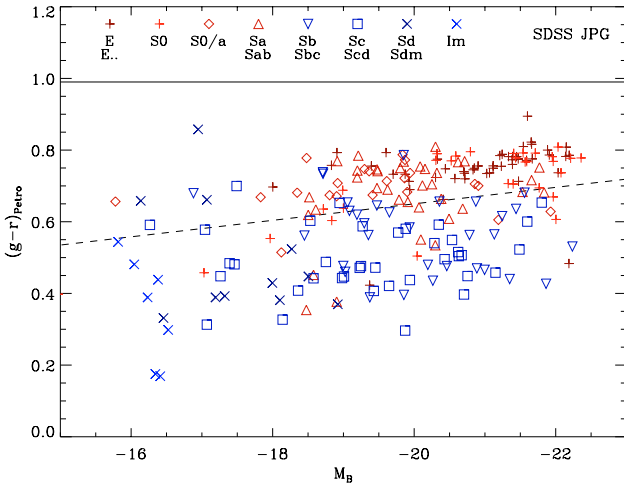
The JPG catalogue includes SDSS photometry and eyeball classifications for 2658 galaxies. This was reduced to 818 galaxies with $r < 15.5$ mag and $z < 0.1$ (median redshift of 0.04). We used the $u - r$ “model” rest-frame colour and a B -band absolute magnitude estimated using the g and r magnitudes. SDSS model magnitudes are based on a fitted profile in the r -band (Stoughton et al. 2002): effectively they are centrally weighted colours. Figure A.1 (right) shows the CMD for these data after sampling to obtain a maximum of 25 galaxies per 0.5-mag bin. The data are divided into eight classification groups (note that an intermediate classification, e.g. Sab, represents an average between two or more classifiers).

The dashed line in Fig. A.1 represents the best-fit dividing line defined by Baldry et al. (2006). This was determined from a significantly larger SDSS sample. This appears to fall in about the right place for the NFGS despite the different colour determination. The faint-end of the red sequence is sparsely populated because these are field samples. In order to compare late-type and blue-sequence derived luminosity functions, we determined the fraction of galaxies on the blue sequence (f_b) for the eight morphological groups. This is shown in Table A.1.

When comparing f_b it should first be noted that the NFGS and JPG samples were selected using different criteria. For example, the JPG sample is r -band magnitude limited and there was no explicit removal of galaxies in high-density regions. Therefore, it is not surprising that the overall f_b is lower. Another factor is the higher median redshift of the JPG which affects the quality of morphological classification (at moderate imaging resolution of $\sim 2''$). For the purposes of this paper the most important difference is the f_b fraction for the Sb, bc galaxies

Table A.1. Fraction of blue-sequence galaxies for different morphological types.

Morphological group	NFGS		SDSS JPG		
	No.	f_b	No.	$f_b(A)$	$f_b(B)$
E	17	0.24	201	0.04	0.03
S0	28	0.21	114	0.18	0.11
S0/a	12	0.42	73	0.19	0.22
Sa, ab	21	0.52	131	0.35	0.37
Sb, bc	31	0.81	152	0.61	0.73
Sc, cd	45	0.93	121	0.86	0.92
Sd, dm	18	0.94	12	0.83	0.75
Im	22	1.00	10	0.90	1.00
all	194	0.68	814	0.37	0.40

(A) using cut in $(u-r)_{\text{model}}$ CMD, (B) using cut in $(g-r)_{\text{Petrosian}}$ CMD.**Fig. A.2.** Morphological classifications in the CMD for galaxies. As per Fig. A.1 (right) except using $g-r$ Petrosian colours instead of $u-r$ model colours. The dashed line represents an optimal divider determined by eye from a larger SDSS sample: $(g-r)_{\text{divide}} = 0.65 - 0.023(M_b + 20)$.

because of their high contribution to the SFR density, as found in Sect. 5.2. This value is 0.61 for the JPG sample (compared to 0.81 for the NFGS). This may partly account for the lower SFR density derived from the blue-sequence SDSS luminosity function (Sect. 4).

One possible reason for a low f_b value for the Sb-classified JPG galaxies is the use of the $u-r$ model colour, which is centrally weighted. It is generally not reliable to use SDSS u -band magnitudes derived from larger apertures because of Poisson noise and sky subtraction, and an alternative is the $g-r$ Petrosian colour. Figure A.2 shows the $g-r$ CMD for the JPG sample, and

the f_b values are also shown in the final column of Table A.1. The f_b value is now 0.73 for Sb, bc galaxies indicating that aperture choice not surprisingly affects the red and blue sequence classification of these galaxies. Nevertheless, a blue-sequence luminosity function can be regarded as being similar to an Sb-or-later luminosity function because of the cross-over in f_b between Sa and Sb (considering the magnitude-limited JPG sample).

References

- Baldry, I. K., Glazebrook, K., Brinkmann, J., et al. 2004, ApJ, 600, 681
 Baldry, I. K., Balogh, M. L., Bower, R. G., et al. 2006, MNRAS, 373, 469
 Blanton, M. R., Hogg, D. W., Bahcall, N. A., et al. 2003, ApJ, 594, 186
 Blanton, M. R., Lupton, R. H., Schlegel, D. J., et al. 2005a, ApJ, 631, 208
 Blanton, M. R., Schlegel, D. J., Strauss, M. A., et al. 2005b, AJ, 129, 2562
 Brinchmann, J., Charlot, S., White, S. D. M., et al. 2004, MNRAS, 351, 1151
 Davies, J., Phillipps, S., Disney, M., Boyce, P., & Evans, R. 1994, MNRAS, 268, 984
 de Jong, R. S., & Lacey, C. 2000, ApJ, 545, 781
 de Vaucouleurs, G., de Vaucouleurs, A., Corwin, H. G., et al. 1991, Third Reference Catalogue of Bright Galaxies (Berlin, Heidelberg, New York: Springer-Verlag), 1
 Disney, M., & Phillipps, S. 1983, MNRAS, 205, 1253
 Felten, J. E. 1976, ApJ, 207, 700
 Fukugita, M., Nakamura, O., Okamura, S., et al. 2007, AJ, 134, 579
 Galaz, G., Villalobos, A., Infante, L., & Donzelli, C. 2006, AJ, 131, 2035
 Gallego, J., Zamorano, J., Aragon-Salamanca, A., & Rego, M. 1995, ApJ, 455, 1
 Gehrels, N. 1986, ApJ, 303, 336
 Hanish, D. J., Meurer, G. R., Ferguson, H. C., et al. 2006, ApJ, 649, 150
 Helmboldt, J. F., Walterbos, R. A. M., Bothun, G. D., O’Neil, K., & de Blok, W. J. G. 2004, ApJ, 613, 914
 Hopkins, A. M., & Beacom, J. F. 2006, ApJ, 651, 142
 Huchra, J., Davis, M., Latham, D., & Tonry, J. 1983, ApJS, 52, 89
 James, P. A., Shane, N. S., Beckman, J. E., et al. 2004, A&A, 414, 23
 James, P. A., Shane, N. S., Knapen, J. H., Etherton, J., & Percival, S. M. 2005, A&A, 429, 851
 Jansen, R. A., Fabricant, D., Franx, M., & Caldwell, N. 2000, ApJS, 126, 331
 Kennicutt, R. C. 1998, ARA&A, 36, 189
 Lauberts, A. 1982, ESO/Uppsala survey of the ESO(B) atlas (Garching: European Southern Observatory (ESO))
 Liske, J., Lemon, D. J., Driver, S. P., Cross, N. J. G., & Couch, W. J. 2003, MNRAS, 344, 307
 Marinoni, C., Monaco, P., Giuricin, G., & Costantini, B. 1999, ApJ, 521, 50
 Nilson, P. 1973, Uppsala general catalogue of galaxies, Acta Universitatis Upsaliensis, Nova Acta Regiae Societatis Scientiarum Upsaliensis, Uppsala Astronomiska Observatoriums Annaler, Uppsala: Astronomiska Observatorium
 Pérez-González, P. G., Gallego, J., Zamorano, J., et al. 2003, ApJ, 587, L27
 Salpeter, E. E. 1955, ApJ, 121, 161
 Santiago, B. X., Strauss, M. A., Lahav, O., et al. 1996, ApJ, 461, 38
 Schechter, P. 1976, ApJ, 203, 297
 Schechter, P. L. 1980, AJ, 85, 801
 Schmidt, M. 1968, ApJ, 151, 393
 Stoughton, C., Lupton, R. H., Bernardi, M., et al. 2002, AJ, 123, 485
 Strateva, I., Ivezić, Ž., Knapp, G. R., et al. 2001, AJ, 122, 1861
 Sullivan, M., Treyer, M. A., Ellis, R. S., et al. 2000, MNRAS, 312, 442
 Tresse, L., & Maddox, S. J. 1998, ApJ, 495, 691